

Article

Experimental Study on the Damping Effect of Multi-Unit Particle Dampers Applied to Bracket Structure

Hang Ye ^{1,2}, Yanrong Wang ^{1,2}, Bin Liu ³ and Xianghua Jiang ^{1,2,*}¹ School of Energy and Power Engineering, Beihang University, Beijing 100191, China² Collaborative-Innovation Center for Advanced Aero-Engine, Beijing 100191, China³ Center for Assessment and Demonstration Research, Academy of Military Sciences, Beijing 100091, China

* Correspondence: jxh@buaa.edu.cn

Received: 29 June 2019; Accepted: 18 July 2019; Published: 20 July 2019

**Featured Application:** Particle dampers have broad application prospects in aerospace equipment and buildings.

Abstract: Particle damping (PD) is a passive mean of vibration control in which small metallic or ceramic particles are placed inside a cavity that attached to the primary structure at the place of high vibration amplitudes. The kinetic energy of the primary structure is dissipated by non-elastic impact and friction between particles and walls. This paper represents a series of experimental investigations of the effects of multi-unit particle dampers (MUPD) attached to a bracket structure under harmonic excitation and random excitation. As a platform to investigate the particle damping characteristics under extreme acceleration environments, the bracket structure was featured by an extremely high response on the top, and its maximum acceleration exceeds 50 times gravity acceleration when the bracket structure was subjected to resonance. This broad range of acceleration conditions was far beyond the scope concerned in most previous work. The experimental results show that for a small weight penalty (no more than 8.8%), multi-unit particle damper can reduce the resonance of the primary structure by more than 50%, whether under sinusoidal excitation or random excitation. And the response of the primary structure depends on the type of cavities and filled coefficient. Layering the cavity in the direction of the main vibration can improve the damping capacity of the multi-unit particle damper. And the damper with small particle size and large number of features is suitable for vibration reduction under high acceleration conditions.

Keywords: multi-unit particle dampers (MUPD); sinusoidal excitation; random excitation; bracket structure

1. Introduction

Particle damping (PD) is a passive means of vibration control in which small metallic or ceramic particles are placed inside a cavity that attached to the primary structure at the place of high vibration amplitudes. The kinetic energy of the primary structure is dissipated by non-elastic impact and friction between particles and walls.

In the 1930s, a primary PD technology—impact damping—was first used by Pagat [1] to attenuate the vibration of the turbine blade. Considering this kind of damper produced large impact noise and was susceptible to the design parameters, some modified dampers were successively introduced. According to the number of units and particles, PD can be classified into four categories [2,3]: impact damper [4], multi-unit impact damper [5], non-obstructive particle damper [6,7] and multi-unit particle damper [8], as shown in Figure 1.

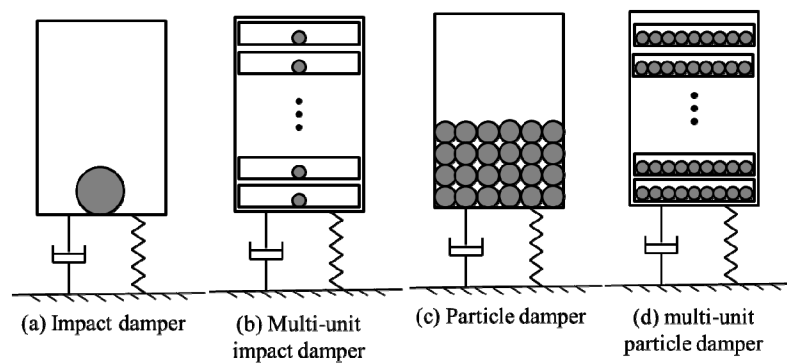


Figure 1. Classification of particle dampers.

Masri [5] first proposed an improved method of a multi-unit single-particle damper, replacing one impact damper with multiple impact dampers to reduce the impact of the single-particle damper.

Many researches have indicated that particle dampers are highly effective in suppressing resonant structural vibration over a wide range of frequencies: Several modes of vibration can be damped simultaneously by one damper design. Experiments conducted by Lieber [4] showed that PD could effectively suppress the wings flutter and general mechanical vibration. Kielb [9] also successfully applied PD to a GE-XTE45 fan blade. Panossian [6] used it to damp the vibration in the liquid oxygen (LOX) inlet tee of a Space Shuttle Main Engine (SSME) and found that PD technology had a good damping efficiency in the high frequency range between 3000 Hz to 6000 Hz. Xu et al. [10] managed to reduce the vibration levels of a desk-top banknotes processing machine by about 40 dB in the range of 2000 Hz to 6000 Hz. Moreover, to illustrate the application of PD in cryogenic temperature environment, Moore et al. [11] performed a series of experimental studies on an impact damper and applied this technique to damp the lateral shaft vibration in a rocket engine turbo pump, where most conventional dampers would be invalid.

To gain an appreciation of the important parameters that may influence the performance of particle damper, most PD experiments were conducted on a cantilever beam with particle dampers. The parameters concerned usually included the type, shape, and size of the particles, the volume fraction, damper location, and the level of excitation. It is found that the factors mentioned above have different effects on particle damping. Some of them, moreover, interconnect with each other. Holikamp and Gordon [12] summarized their experimental findings that the damper was strongly dependent upon vibration amplitude, damper location, and mass of particles. Friend and Kinra [13] further pointed out the key aspect for amplitude dependent behavior under gravity was the particles' acceleration characteristics. Although these studies have highlighted the basic rules of particle damping, the acceleration response range, given the cantilever beam structure, is relatively limited for practical application.

Saeki and Masri laid foundational analytical methods for mechanism research on a single-unit multi-particle damper [5,14–16]. But the research on multi-unit particle dampers (MUPDs) is still in its infancy. In 2005, Saeki [8] first gave the definition of multi-unit particle damper, and studied the influence of the number of units and cavity size on particle damping with the single-degree-of-freedom system of horizontal vibration. Since the multi-unit particle damper in the literature is in the same response environment, Saeki assumed that the damping effect of the multi-body particle damper was actually a linear superposition of single-unit multi-particle damper. Through the discrete element method (DEM) and experimental approaches, the damping mechanism of MUPDs under different excitations was studied in detail by Lu [17–21]. The research object involved in this paper is a bracket structure with a particle damper located at a large vibration amplitude position, which provides an appropriate platform to study the characteristics of particle damping in the high vibration amplitude (acceleration higher than 50 times gravity acceleration) and the feasibility of applying multi-unit

particle dampers to a relatively complex structure. The effects of damper cavity, collision clearance, type, and size of particle were investigated under harmonic excitation and random excitation.

2. Experimental Setup and Scheme

2.1. Experimental Structure and Setup

The experimental structure, illustrated in Figure 2, consisted of a base, a bracket, and a wheel. It is a component in the spacecraft and made from aluminum alloy. The primary structure mass is 11.07 kg. Figure 2a illustrates the Cartesian coordinates definition of the primary structure. The vertical direction is defined as the Z, the axis direction of the wheel is defined as the Y, and the direction perpendicular to the Z and Y directions is defined as the X.

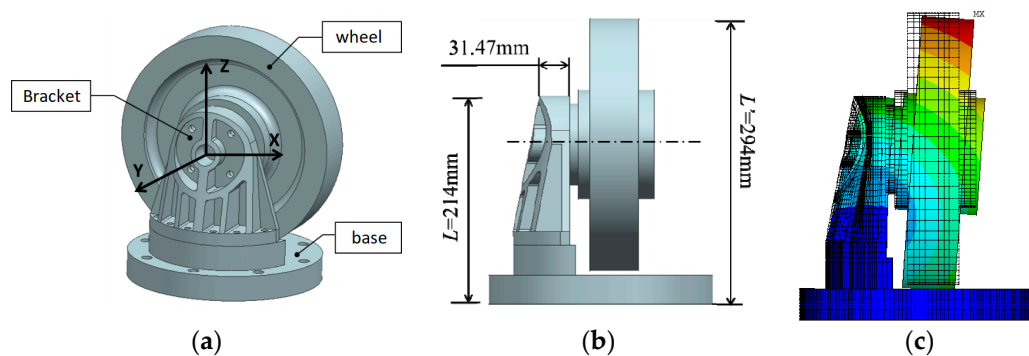


Figure 2. Test structure (a) coordinate definition and component name; (b) structure size; (c) fundamental mode shape of the primary system.

The natural frequency of the fundamental mode of the primary structure is $f_n = 240$ Hz. The fundamental mode shape is shown in Figure 2c. It was known by modal identification that the corresponding mode was first-order bending mode of the primary structure, and the main response is in the Y direction.

According to [22–24], for achieving high damping, the damper should be installed on a large displacement position to acquire the vigorous impact of particles. The multi-unit particle damper was installed on the top of the bracket and the particle cavities connected to the bracket by an adapter, as shown in Figure 3.

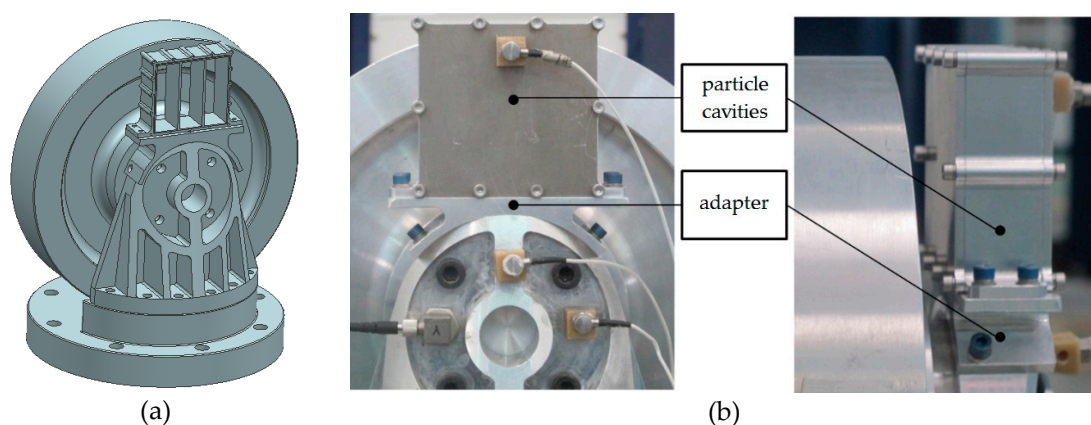


Figure 3. Connection scheme of particle cavities with the primary structure. (a) bracket structure; (b) test model.

The multi-unit particle damper was made of aluminum alloy plates consisting of three rectangular containers, in which the walls in the Y direction can be removed to add particles. The cavity types

and internal dimensions used in this study are listed in Table 1. All cavities are equally divided into 3 sub-cavities along the X direction, as shown in Figure 3. The serial number of the cavity indicates that the number of layers along the Y and Z directions is different: The A-cavity has no layering in the Z direction, and the Z-direction height of the cavity is 64 mm. The B-cavity is divided into 2 layers in the Z direction, and the height of each sub-chamber is 31 mm (the partition thickness is 2 mm). The C-cavity is divided into 5 layers in the Z direction, and the Z-direction height of each sub-chamber is 11.2 mm. According to whether it is layered in the Y direction (the main response direction of the bracket), the above-mentioned cavity of each type is further divided into two types. The suffix number “1” indicates that the Y direction is not layered, that means the Y-direction dimension of a single sub-cavity is 28 mm. And the suffix number “2” indicates that the Y-direction is divided into two layers, and the single sub-cavity Y-direction dimension is 14 mm. The horizontal direction of the cross-sectional view in Table 1 is the Y direction, and the vertical direction is the Z direction. The modal analysis of the A1 cavity can be achieved under the condition that the bottom mounting hole is fixed, the first-order modal frequency is 1993, 6 Hz, and the main vibration direction is Y-direction. This means that the damper cavity stiffness is large enough to have a negligible effect on the first-order bending frequency of the primary structure.

Table 1. Random excitation loading conditions.





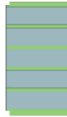
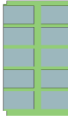
Serial Number of the Cavity	A1	A2	B1	B2	C1	C2
Sub-cavity size X × Y × Z (mm)	22 × 28 × 64	22 × 14 × 64	22 × 28 × 31	22 × 14 × 31	22 × 28 × 11.2	22 × 14 × 11.2
Number of sub-cavities	3	6	6	12	15	18
Total volume of the cavity (mm ³)	118,272	118,272	114,576	114,576	103,488	103,488
A cross-sectional view of the X-direction						

Figure 4 shows a schematic diagram of the experimental apparatus. The multi-unit particle damper was first fixed on a steel pedestal and then firmly connected to the shaker platform. This test system included an LS232-GT500M 2t-level shaker, several m + p Vibpilot-8 controllers and B and W piezoelectric acceleration sensors. The sampling frequency was set to 5.12 kHz. The motion of the primary structure and the base was measured with six accelerometers.

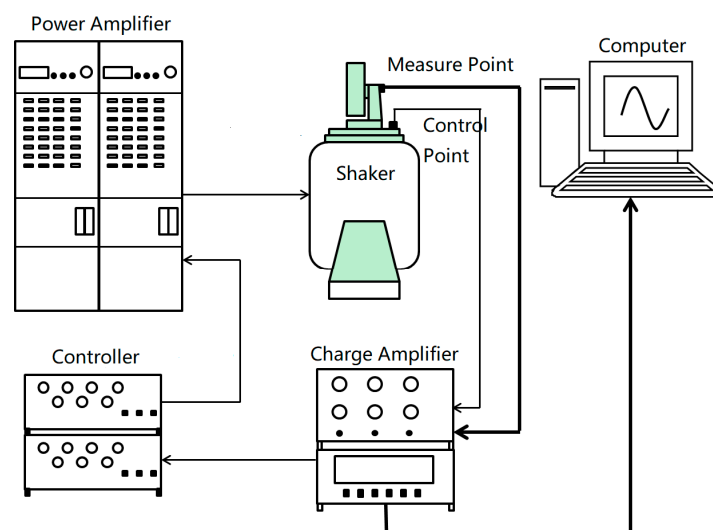


Figure 4. Schematic of experimental apparatus.

2.2. Experimental Scheme

The particles tested were as follows: 304 stainless steel particles (2 mm diameter) (Defined as Fe in the legend), lead particles (2 mm diameter), stainless steel powder (about 0.048 mm diameter), tungsten carbide powder (about 0.5 mm diameter), as shown in Figure 5. The density of the chosen material: stainless steel ($7.93 \times 10^3 \text{ kg/m}^3$), lead ($11.3 \times 10^3 \text{ kg/m}^3$) and tungsten carbide ($15.6 \times 10^3 \text{ kg/m}^3$). In practical engineering applications, the mass ratio between the damper and the primary structure should be small, usually no more than 10%. All of the experiments were conducted with additional mass (sum of the adapter, the particle cavity, and particles mass) no more than 1 kg, which corresponds to a mass ratio of 8.8%.

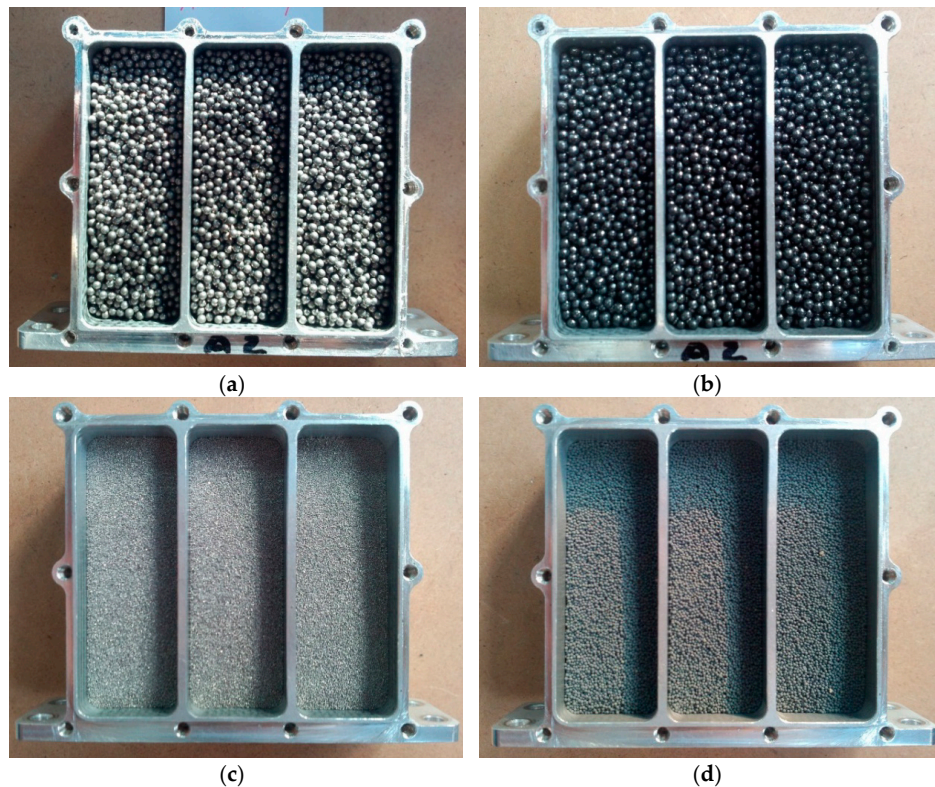


Figure 5. Particle type (a) 304 Stainless steel particles (2 mm diameter); (b) Lead particles (2 mm diameter); (c) Stainless steel powder (about 0.048 mm diameter); (d) Tungsten carbide powder (about 0.5 mm diameter).

The loading conditions of the standard sine sweep were described as follows: the acceleration was maintained 1 g the scope of sweeping frequency was from 20 Hz to 1000 Hz, and the sweep rate was set as 2 oct/min. The random excitation loading conditions were shown in Table 2.

Table 2. Random excitation loading conditions.

Frequency Range	Power Spectral Density (g^2/Hz)
10–100	3 dB/oct
100–200	0.08
600–2000	−9 dB/oct
RMS acceleration	8.1 g
Loading time	1 min
Loading direction	Z

The primary structure with the adapter was as a reference scheme (Figure 6), numbered Sup_1. Figure 7 showed the response of the main structure of Sup_1. Consistent with the modal analysis results in Section 2.1, the maximum response direction of the primary structure for the fundamental mode shape is Y direction, and the value is about 68 g.

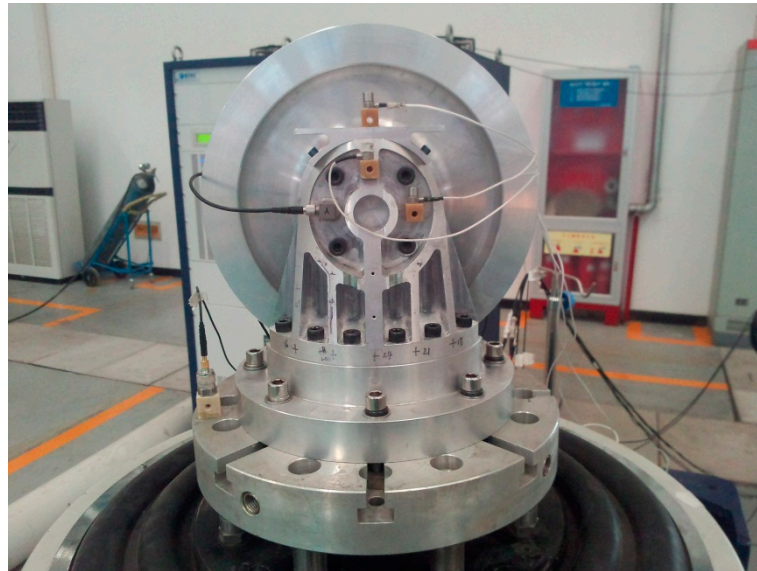


Figure 6. Configuration of the reference scheme.

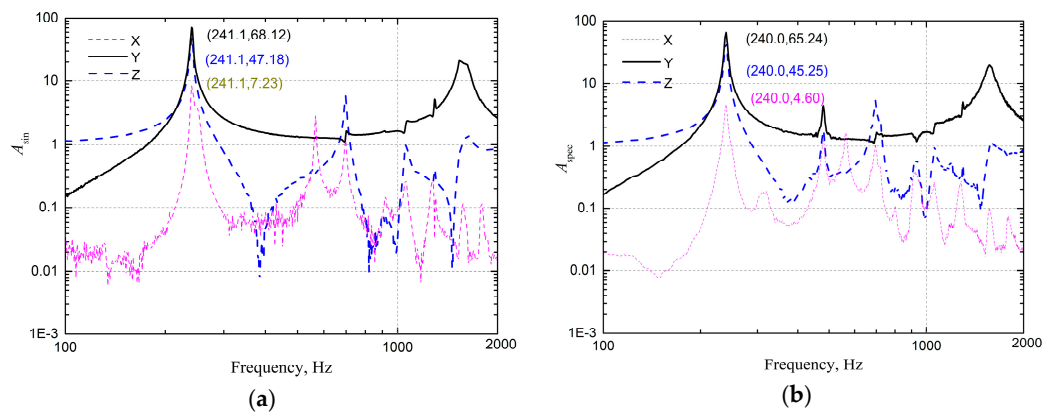


Figure 7. The frequency response function of Sup_1: (a) Sinusoidal excitation; (b) Random excitation.

3. Experimental Results

Due to the slight difference in the internal volume of the damper cavities, the particle filling factor V_r is defined as the maximum number of particles contained in a single sub-cavity in a C2 cavity is set as a filling factor $V_r = 1$. The mass of a single cavity filling of particles with different particle sizes at $V_r = 1$ is shown in Table 3. It should be noted that the maximum filling of the A and B cavities corresponds to a V_r greater than 1, which is about 1.14.

Table 3. Particle mass ($V_r = 1$, C2 Cavity).

Particle Type	2 mm Stainless Steel Particles	2 mm Lead Particles	300 Mesh Stainless Steel Powder	32 Mesh Tungsten Carbide Powder
Particle mass (g)	15.28	21.09	15.89	24.55

3.1. Control Experiment

The mass of particle cavities is slightly different. It is well known that the damper mass is an important factor affecting the damping effect, and the connection bolts between the cavity and the adapter may also affect the structural response. This section evaluates the effect of two factors on the test and compares the primary structure measurements with different cavities to the control scheme in Table 4. “Without cover” in the table means that the cover on both sides of the cavity is not installed.

Table 4. Mass of each component.

Component Name	Mass (g)
Primary structure	11070
A1 cavity	110
A2 cavity	151
B1 cavity	123
B2 cavity	161
C1 cavity	160
C2 cavity	198
Cover	24
Adapter	70

As shown in Table 5, the damper cavity has little effect on the response of the primary structure. The resonant frequency of the primary structure with the adapter and the damper cavity is slightly reduced. The amplification factor of the main structure with the particle cavity installed has a slightly reduced under sinusoidal excitation and random excitation conditions, but the variation amplitude is within 10%.

Table 5. The effect of the cavity and the adapter: (a) Sinusoidal excitation; (b) Random excitation.

(a)					
Scheme Name	Additional Mass (g)	Additional Total Mass (Including Adapter) (g)	f_{sin}	A_{sin}	
Sup_1	0	70	240.81	71.53	
A1 (without cover)	110	180	237.80 (−1.25%)	68.30 (−4.52%)	
A1	158	228	236.89 (−1.63%)	68.20 (−4.66%)	
C1	208	278	233.42 (−3.07%)	64.24 (−10.19%)	
C2 (without cover)	198	268	235.20 (−2.33%)	66.39 (−7.19%)	
C2	246	316	231.49 (−3.87%)	65.89 (−7.88%)	

(b)					
Scheme Name	Additional Mass (g)	Additional Total Mass (Including Adapter) (g)	f_{spec}	Grms	A_{spec}
Sup_1	0	72	240.00	48.48	62.73
A1 (without cover)	110	180	235.99 (−1.67%)	47.23 (−2.58%)	60.13 (−4.14%)
A1	158	228	234.00 (−2.50%)	46.02 (−5.07%)	59.34 (−5.40%)
C1	208	278	232.01 (−3.33%)	44.26 (−8.70%)	57.17 (−8.86%)
C2 (without cover)	198	268	234.00 (−2.50%)	44.27 (−8.68%)	58.81 (−6.25%)
C2	246	316	232.01 (−3.33%)	43.35 (−10.58%)	56.78 (−9.49%)

It can be observed from experiments that only the damping change caused by the additional concentrated mass is small, and the main cause of the structural response change is several bolt connections between the end cap and the cavity. Therefore, in the subsequent tests, the screws at the joints were tightened with a constant torque electric screwdriver.

3.2. Effect of Layering in Z-Direction of the Cavity

The purpose of layering the cavity in the Z-direction of is to prevent the particles/powder from accumulating under the action of gravity, to enhance the movement ability of the underlying particles/powder, and on the other hand, to adjust the collision gap between the particles and the cavity in the Z direction.

The number of Z-direction layers corresponding to the cavities A1, B1, and C1 are 1, 2, and 5, respectively, and the Z-direction collision gaps of B1 and C1 are 1/2 and 1/5 of A1, respectively.

This part of the test was carried out with 2 mm stainless steel particles and 32 mesh tungsten carbide powder. The test results are shown in Table 6. The amplitude–frequency response curves corresponding to Table 6 are shown in Figures 8 and 9.

Table 6. Effect of layering in Z-direction of the cavity.

Scheme Name	Sinusoidal Excitation		Random Excitation		
	f_{sin}	A_{sin}	f_{spec}	Grms	A_{spec}
Sup_1	240.81	71.53	240.00	48.48	62.73
A1_Fe_0.9	236.81 (−1.66%)	39.91 (−44.21%)	235.01 (−2.08%)	37.02 (−23.64%)	43.67 (−30.39%)
B1_Fe_0.9	235.70 (−2.12%)	43.23 (−39.57%)	234.00 (−2.50%)	44.02 (−26.61%)	50.34 (−40.10%)
C1_Fe_0.9	234.72 (−2.53%)	41.63 (−41.80%)	232.01 (−2.50%)	42.26 (−30.72%)	47.17 (−46.50%)
A1_WC_0.9	235.05 (−2.39%)	9.80 (−86.30%)	234.00 (−1.67%)	44.27 (−36.20%)	52.81 (−52.14%)
B1_WC_0.9	235.70 (−2.12%)	32.89 (−54.02%)	232.01 (−2.08%)	40.35 (−31.42%)	44.78 (−46.29%)
C1_WC_0.9	233.61 (−2.99%)	31.77 (−54.19%)	234.00 (−2.50%)	32.58 (−32.79%)	30.74 (−50.99%)

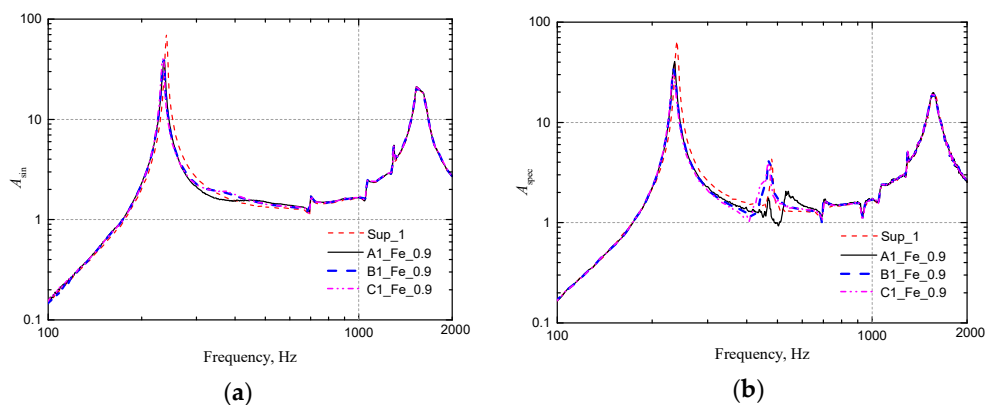


Figure 8. Experiment results of 2 mm stainless steel particle (layering in Z-direction of the cavity): (a) Sinusoidal excitation; (b) Random excitation.

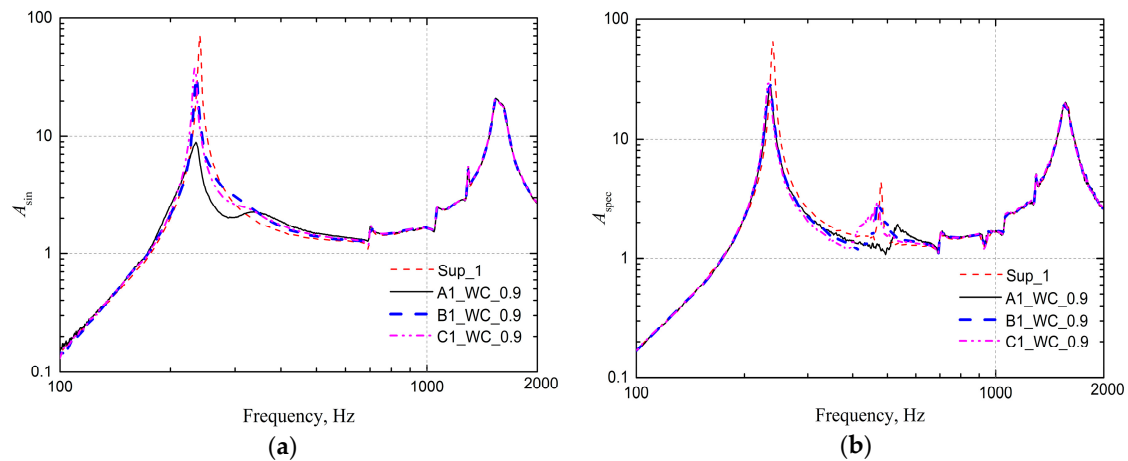


Figure 9. Experiment results of Tungsten carbide powder (layering in Z-direction of the cavity); (a) Sinusoidal excitation; (b) Random excitation.

The structural frequency variation caused by different Z-direction layering schemes is within 3%; the best solution for damping effect of stainless steel particles is C1_304_0.9, which corresponds to a decrease of 41.8% for the measuring point response amplification factor A_{sin} , and A_{spec} decreases 46.5%; The best solution for tungsten carbide powder is A1_WC_0.9, which corresponds to a decrease of 86.30% for A_{sin} , and a decrease of 52.14% for A_{spec} .

The test results show that for 2 mm stainless steel particles, Z-direction stratification is beneficial to improve the damping effect of stainless steel particles. The more Z-layers, the lower the response peak. However, from the perspective of the variation of the RMS value, the promotion effect of layering is not obvious. The Z-direction layering has some negative effects on the tungsten carbide powder. The Z-direction layering of the cavity under sinusoidal excitation reduces the particle damping, while the layering has no obvious influence on the particle damping under random excitation. In view of the above results, it is not recommended to layer the cavity in the Z-direction.

3.3. Effect of Layering in the Y-Direction of the Cavity

Since the main response direction of the structure is the Y direction, the Y-direction collision gap between the particles and the cavity is particularly concerned.

The “2” type cavity (cavity with spacers in the Y direction) can ensure that the Z-direction collision gap is equal to the “1” type cavity (Y-direction non-separator), and the Y-direction collision gap is reduced to half. In this part of the test, the C1 and C2 cavities were first used to test 2 mm stainless steel particles and 32 mesh tungsten carbide powder. The test results are shown in Table 7, and the corresponding amplitude–frequency response curve are Figures 10 and 11.

It can be seen that the best damping effect in the Y-stratified scheme is C2_WC_0.9, and the response peaks A_{sin} and A_{spec} of the main structure are decreased by 56.23% and 63.20%, respectively, and the frequency change caused by the damper is also the largest. The modal frequency was reduced by 3.41%. The C2_304_0.9 filled with stainless steel particles also achieved good damping effect, and A_{sin} and A_{spec} reductions also reached 60.77% and 68.13%, respectively.

The experimental results showed that layering in Y-direction is beneficial to the improvement of the UMPD damping effect. When the particle mass is kept constant, the response amplitude can be further attenuated by 20 to 30% through layering the cavity in Y-direction.

Table 7. Effect of layering in Y-direction of the cavity.

Scheme Name	Sinusoidal Excitation		Random Excitation		
	f_{sin}	A_{sin}	f_{sepc}	Grms	A_{sepc}
Sup_1	240.81	71.53	240.00	48.48	62.73
C1_304_0.9	234.72 (−2.53%)	41.63 (−41.80%)	234.00 (−2.50%)	33.59 (−30.72%)	33.56 (−46.50%)
C2_304_0.9	233.61 (−2.99%)	28.06 (−60.77%)	233.33 (−2.78%)	29.70 (−38.73%)	23.37 (−62.74%)
C1_WC_0.9	233.61 (−2.99%)	37.77 (−47.19%)	234.00 (−2.50%)	32.58 (−32.79%)	30.74 (−50.99%)
C2_WC_0.9	232.60 (−3.41%)	31.31 (−56.23%)	234.00 (−2.50%)	29.78 (−38.58%)	23.08 (−63.20%)

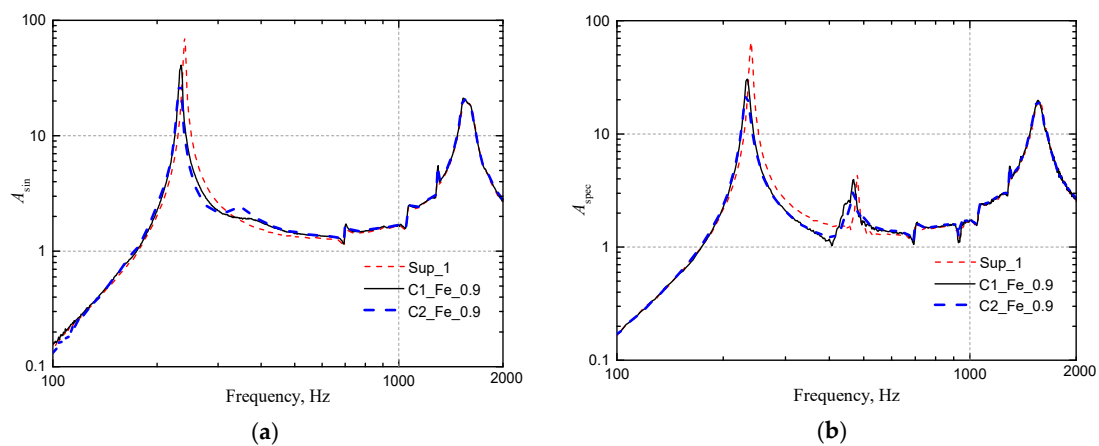


Figure 10. Experiment results of 2 mm stainless steel particle (layering in Y-direction of the cavity): (a) Sinusoidal excitation; (b) Random excitation.

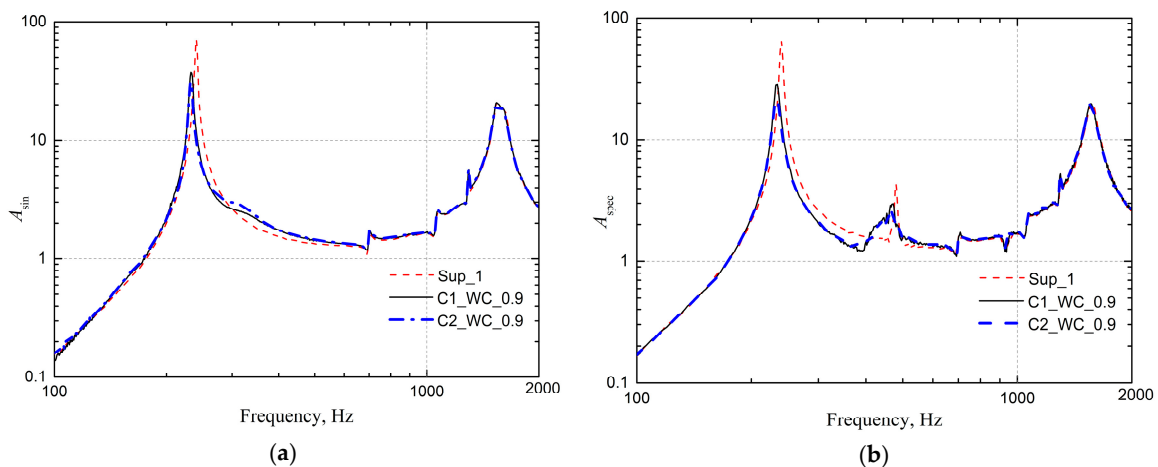


Figure 11. Experiment results of Tungsten carbide powder (layering in Y-direction of the cavity); (a) Sinusoidal excitation; (b) Random excitation.

Two-millimeter lead and stainless steel particles and tungsten carbide powder were filled into the A1 and A2 cavities, respectively, and the test results were compared to verify the speculation about the optimal cavity. The test results are shown in Table 8, and the corresponding measurement lines are shown in Figures 12–14. The same trend as given in Table 7, it can be seen that the damping effect of the A2 scheme continues to increase on the basis of A1, so that the A_{sin} and A_{spec} of the schemes A2_Pb_0.9

and A2_304_0.9 are respectively reduced by the A1 cavity. Forty-seven point four two percent, 44.21% increased to 75.13%, 47.53%. Therefore, it can be determined that the optimum cavity is A2.

Table 8. Optimal cavity analysis.

Scheme Name	Sinusoidal Excitation		Random Excitation		
	f_{sin}	A_{sin}	f_{spec}	Grms	A_{spec}
Sup_1	240.81	71.53	240.00	48.48	62.73
A1_Pb_0.9	236.07 (−1.97%)	37.61 (−47.42%)	234.00 (−2.50%)	33.84 (−30.19%)	34.43 (−45.12%)
A2_Pb_0.9	234.69 (−2.54%)	17.79 (−75.13%)	234.00 (−2.50%)	29.56 (−39.03%)	24.44 (−61.04%)
A1_304_0.9	236.81 (−1.66%)	39.91 (−44.21%)	235.01 (−2.08%)	37.02 (−23.64%)	43.67 (−30.39%)
A2_304_0.9	234.69 (−2.54%)	37.53 (−47.53%)	234.00 (−2.50%)	32.28 (−33.42%)	28.84 (−54.03%)
A1_WC_0.9	235.03 (−2.40%)	9.74 (−86.39%)	235.99 (−1.67%)	31.10 (−35.84%)	28.32 (−54.86%)
A2_WC_0.9	227.40 (−5.57%)	6.79 (−90.51%)	234.00 (−2.50%)	25.70 (−46.99%)	13.91 (−77.82%)

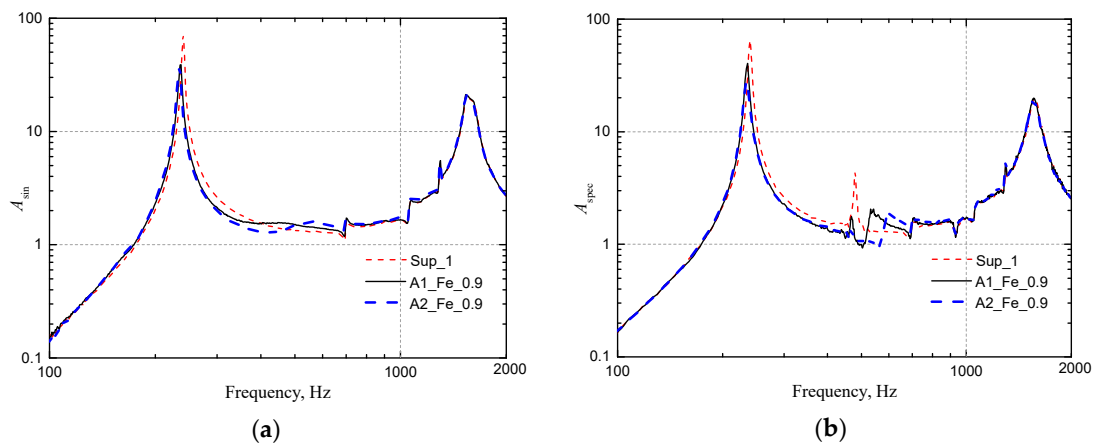


Figure 12. Experiment results of 2 mm stainless steel particles for A1 and A2 cavity (layering in Y-direction of the cavity): (a) Sinusoidal excitation; (b) Random excitation.

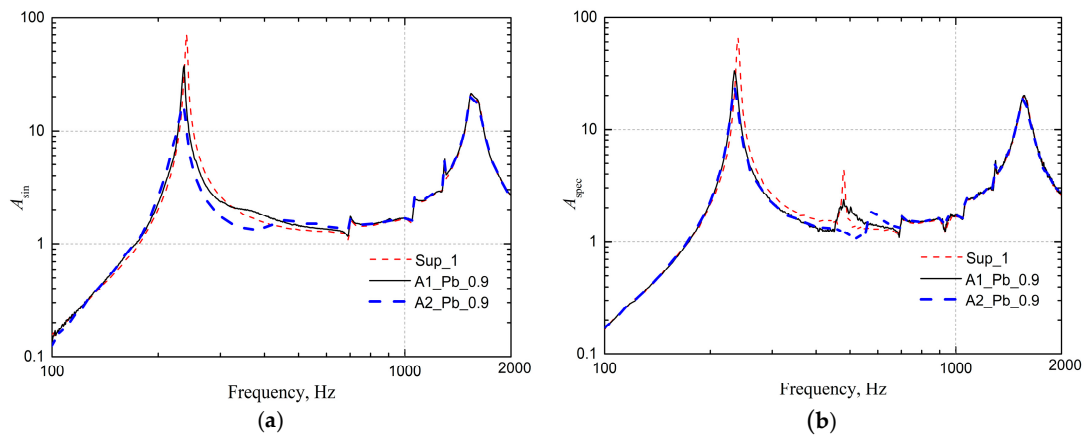


Figure 13. Experiment results of 2 mm lead particles for A1 and A2 cavity (layering in Y-direction of the cavity): (a) Sinusoidal excitation; (b) Random excitation.

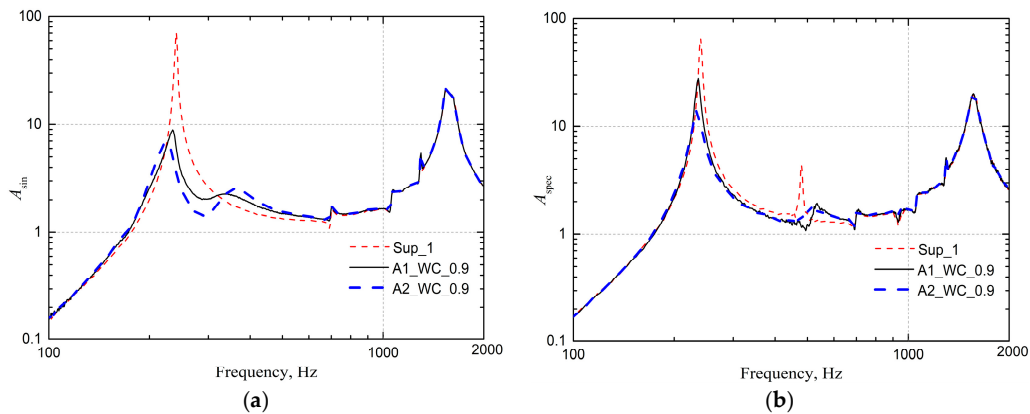


Figure 14. Experiment results of Tungsten carbide powder for A1 and A2 cavity (layering in Y-direction of the cavity): (a) Sinusoidal excitation; (b) Random excitation.

3.4. Effect of Particle/Powder Material

Particle/powder material is an important factor affecting particle damping. The difference includes material density, particle surface hardness, and friction coefficient.

This section compares four kinds of particles or powder, which are 2 mm stainless steel particles, lead particles, stainless steel powder, and tungsten carbide powder.

The A1 cavity was adopted to test the selected particles and powder. The filling factor V_r is 0.9, the results are shown in Table 9, and the corresponding amplitude–frequency responses are shown in Figures 15 and 16. It can be seen that the lead-filled particles are superior to the stainless steel particles in damping, especially under random excitation conditions, the former (−45.12%) is 50% lower than the latter (−30.39%). For the lead particles, the response peak A_{sin} and A_{spec} reduction amplitudes are 47.42% and 45.12%, respectively. Therefore, 2 mm lead particles can be used as an alternative to the best granular material. Compared with stainless steel powder and tungsten carbide powder, tungsten carbide powder is obviously dominant under sinusoidal excitation, A_{sin} is reduced by 86.30%, slightly dominated under random conditions, and A_{spec} is reduced by 52.14%.

Therefore, tungsten carbide powder can be used as an alternative to the best powder filling material. In summary, the tungsten carbide powder has the best vibration damping effect, followed by stainless steel powder, 2 mm lead particles, and stainless steel particles had the worst vibration damping effect.

Table 9. Effect of particle/powder material.

Scheme Name	Harmonic Excitation		Random Excitation		
	f_{sin}	A_{sin}	f_{spec}	Grms	A_{spec}
Sup_1	240.81	71.53	240.00	48.48	62.73
A1_Fe_0.9	236.81 (−1.66%)	39.91 (−44.21%)	235.01 (−2.08%)	37.02 (−23.64%)	43.67 (−30.39%)
A1_Pb_0.9	236.07 (−1.97%)	37.61 (−47.42%)	234.00 (−2.50%)	33.84 (−30.19%)	34.43 (−45.12%)
A1_Fe (p)_0.9	235.70 (−2.12%)	32.06 (−55.18%)	234.00 (−2.50%)	32.42 (−33.13%)	31.58 (−49.65%)
A1_WC_0.9	235.05 (−2.39%)	9.80 (−86.30%)	235.99 (−1.67%)	30.93 (−36.20%)	30.02 (−52.14%)

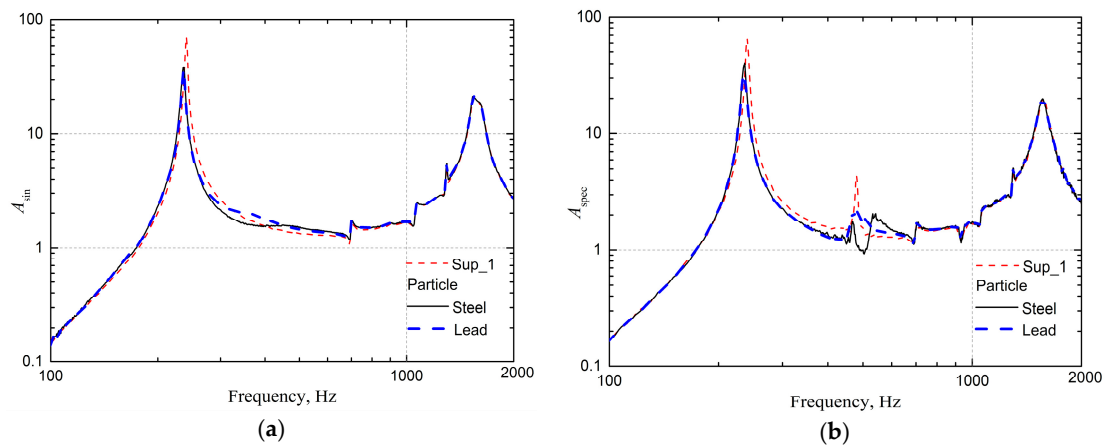


Figure 15. Experiment results of particle material: (a) Sinusoidal excitation; (b) Random excitation.

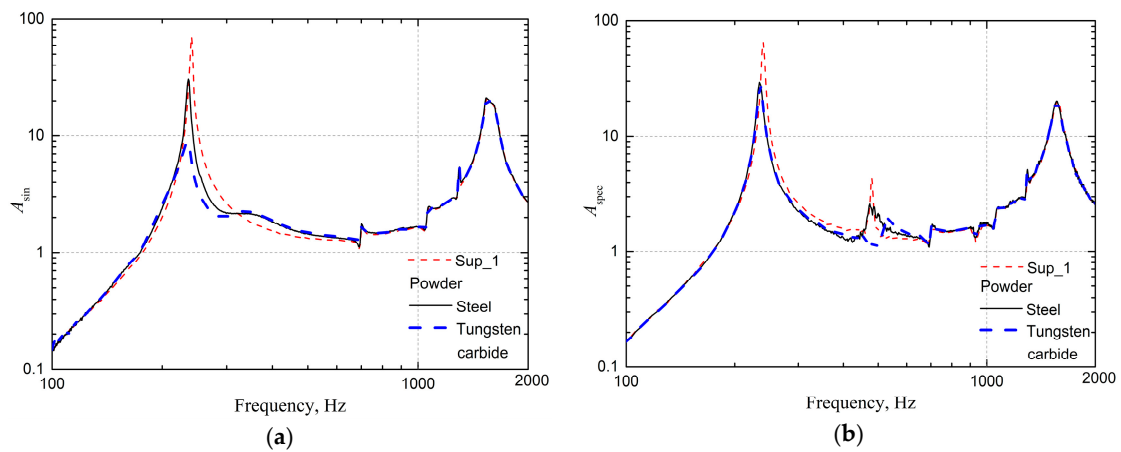


Figure 16. Experiment results of powder material: (a) Sinusoidal excitation; (b) Random excitation.

3.5. Effect of the Filling Coefficient

For the C2 cavity, the maximum filling coefficient $V_r = 1$, and for the A1/A2 cavity, the maximum filling coefficient $V_r = 1.14$. In this part of the experiment, the filling coefficient of tungsten carbide powder in the cavity of A1 and A2 was adjusted to obtain the influence law and the corresponding optimal filling coefficient. The additional mass of each damper scheme is shown in Table 10. The corresponding test results are shown in Table 11, and the amplitude–frequency response is shown in Figure 17.

Table 10. Tungsten carbide powder mass.

Scheme Name	Cavity Mass (g)	Powder Mass (g)	Additional Total Mass (Including Adapter) (g)
Sup_1	0	0	72
A1_WC_0.9	158	662.85	890.85
A1_WC_0.95	158	699.68	927.68
A1_WC_1.00	158	736.50	964.50
A1_WC_1.05	158	773.325	1001.325
A1_WC_1.10	158	810.15	1038.15

Table 11. Effect of tungsten carbide powder filling coefficient.

Scheme Name	Harmonic Excitation		Random Excitation		
	f_{sin}	A_{sin}	f_{spec}	Grms	A_{spec}
Sup_1	240.81	71.53	240.00	48.48	62.73
A1_WC_0.9	235.03 (−2.40%)	9.74 (−86.39%)	235.99 (−1.67%)	31.10 (−35.84%)	28.32 (−54.86%)
A1_WC_0.95	234.14 (−2.77%)	8.25 (−88.46%)	234.00 (−2.50%)	30.77 (−36.54%)	27.24 (−56.57%)
A1_WC_1.00	231.01 (−4.07%)	6.19 (−91.34%)	235.01 (−2.08%)	29.69 (−38.75%)	23.37 (−62.75%)
A1_WC_1.05	230.46 (−4.30%)	5.09 (−92.88%)	235.01 (−2.08%)	28.68 (−40.85%)	20.75 (−66.92%)
A1_WC_1.10	229.95 (−4.51%)	5.05 (−92.94%)	235.99 (−1.67%)	28.55 (−41.12%)	19.92 (−68.24%)

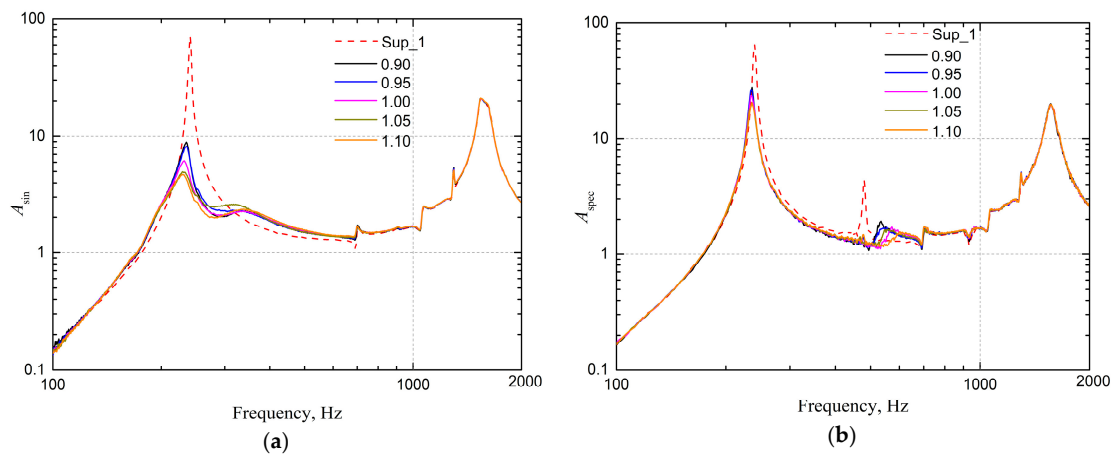


Figure 17. The effect of the filling coefficient on the experiment results: (a) Sinusoidal excitation; (b) Random excitation.

The amplification factor ratio A' is defined as the ratio of the amplification factor to the control scheme in the different experiment scheme. Figure 18 shows the effect of the filling coefficient on the damping effect of the above tungsten carbide filling scheme with the filling coefficient V_r as the abscissa and the magnification factor ratio A' as the ordinate. As can be seen from Figure 17, when the filling coefficient increased to 1.05, A'_{sin} stops decreasing under sinusoidal excitation, and the random excitation decreases slowly, thereby determining that 1.05 is the optimum filling coefficient. The damping effect of the 2 mm particle filling scheme was tested in accordance with the fill factor. Table 12 shows the test results for increasing the filling coefficient of lead and stainless steel particles. It can be seen that increasing V_r helps to improve the damping effect.

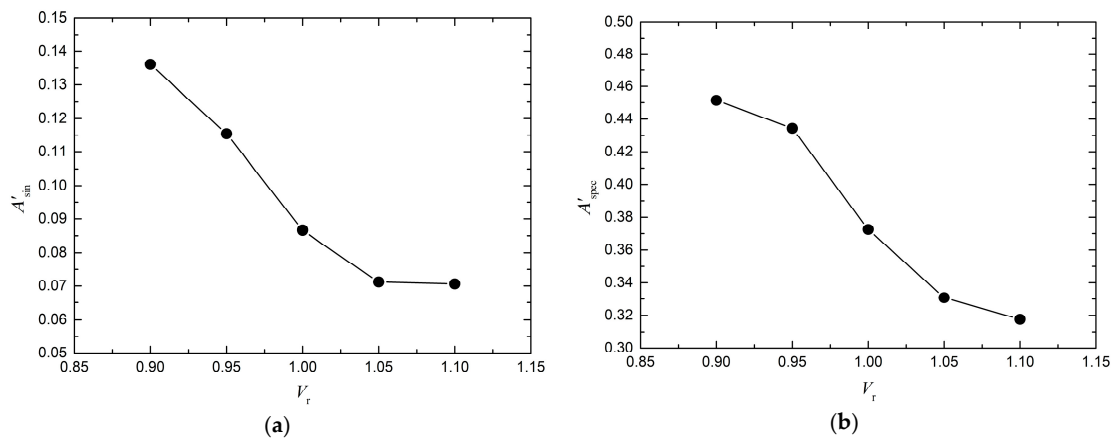


Figure 18. Influence of filling coefficient on the amplitude of amplification coefficient: (a) Sinusoidal excitation; (b) Random excitation.

Table 12. Effect of particle filling coefficient.

Scheme Name	Harmonic Excitation		Random Excitation		
	f_{sin}	A_{sin}	f_{spec}	Grms	A_{spec}
Sup_1	240.81	71.53	240.00	48.48	62.73
A1_Pb_0.9	236.07 (−1.97%)	37.61 (−47.42%)	234.00 (−2.50%)	33.84 (−30.19%)	34.43 (−45.12%)
A1_Pb_1.05	236.07 (−1.97%)	26.88 (−62.42%)	235.99 (−1.67%)	32.35 (−33.27%)	29.87 (−52.38%)
A1_Fe_0.9	236.81 (−1.66%)	39.91 (−44.21%)	235.01 (−2.08%)	37.02 (−23.64%)	43.67 (−30.39%)
A1_Fe_1.05	235.73 (−2.11%)	26.03 (−63.61%)	235.34 (−1.94%)	34.65 (−28.53%)	36.52 (−41.79%)

4. Discussion and Conclusions

In this paper, the effects of additional structural quality, Y-direction and Z-direction stratification, particle material, and filling factor of the particle damper on the damping effect are investigated by experiments. The main conclusions are as follows:

- (1) The differences between the resonance frequencies of the primary structure with and without particle dampers are small. For the scheme in which the additional mass (The sum of the mass of the adapter and the particle damper) does not exceed 1000 g and the maximum response of the primary structure can be attenuated by more than 50%, and the first-order frequency of the primary structure decreases most when the A2_WC_0.9 type particle damper is installed, which is 5.57%.
- (2) Layering the cavity in the direction of the main vibration can improve the efficiency of particle damping. This is because the multi-unit damper can increase the number of collisions between the particles and the wall. But in the direction of a small vibration amplitude, layering the damper does not significantly improve the particle damping efficiency.
- (3) With the same filling factor, the tungsten carbide powder has the best damping effect. When the filling coefficient and the cavity is kept constant, the damping effect of the particle damper is positively correlated with the particle density.
- (4) There is an optimal filling coefficient, but the values corresponding to different cavities are slightly different. For the A1 cavity, the optimum filling coefficient for filled tungsten carbide powder, 2 mm lead, and stainless steel particles is 1.05, while for the A2 cavity, the best filling coefficient is 0.9.

The structural shape of the cavity affects the collision between the particles, which in turn affects the energy consumed in a single cycle. The interaction between particles during motion can be found in reference [23].

It should be noted that the optimal damper design was determined in this paper from the trial-and-error method. But the Kalman filter and the Taguchi method are more efficient optimization methods for experimental design [25–27]. In addition, the damper proposed in this paper requires a large installation space and is not suitable for tight structures. For tight structures, multiple small damper combinations are required to achieve vibration damping effect [22]. And the use of a viscoelastic material as a cavity can further increase the damping effect of the damper [28].

Author Contributions: B.L. and Y.W. designed the experiments. B.L. and H.L performed the experiments and analyzed the data. H.Y. wrote the paper. X.J. revised the paper.

Funding: This research was funded by the National Natural Science Foundation of China, grant number 51475022.

Conflicts of Interest: The authors declare no conflicts of interest.

References

1. Paget, A. Vibration in steam turbine buckets and damping by impacts. *Engineering* **1937**, *143*, 305–307.
2. Lu, Z.; Wang, Z.; Masri, S.; Lu, X. Particle impact dampers: Past, present, and future. *Struct. Control Health Monit.* **2017**, *25*, e2058. [[CrossRef](#)]
3. Lu, Z.; Wang, Z.; Zhou, Y.; Lu, X. Nonlinear dissipative devices in structural vibration control: A review. *J. Sound Vib.* **2018**, *423*, 18–49. [[CrossRef](#)]
4. Lieber, P.; Jensen, D. An acceleration damper: Development, design and some applications. *Trans. ASME* **1945**, *67*, 523–530.
5. Masri, S. Analytical and Experimental Studies of Multiple-Unit Impact Dampers. *J. Acoust. Soc. Am.* **1969**, *45*, 1111–1117. [[CrossRef](#)]
6. Panossian, H. Structural damping enhancement via non-obstructive particle damping technique. *J. Vib. Acoust.* **1992**, *114*, 101–105. [[CrossRef](#)]
7. Papalou, A.; Masri, S. Performance of particle dampers under random excitation. *J. Vib. Acoust.* **1996**, *118*, 614–621. [[CrossRef](#)]
8. Saeki, M. Analytical study of multi-particle damping. *J. Sound Vib.* **2005**, *281*, 1133–1144. [[CrossRef](#)]
9. Kielb, R.; Macri, F.G.; Oeth, D.; Nashif, A.; Macioce, P.; Panossian, H.; Lieghley, F. Advanced damping systems for fan and compressor blisks. In Proceedings of the 34th AIAA/ASME/SAE/ASEE Joint Propulsion Conference and Exhibit, Cleveland, OH, USA, 13–15 July 1998.
10. Xu, Z.; Wang, M.Y.; Chen, T. A particle damper for vibration and noise reduction. *J. Sound Vib.* **2004**, *270*, 1033–1040. [[CrossRef](#)]
11. Moore, J.J.; Palazzolo, A.B.; Gadangi, R.; Nale, T.A.; Klusman, S.A.; Brown, G.V.; Kascak, A.F. A forced response analysis and application of impact dampers to rotordynamic vibration suppression in a cryogenic environment. *J. Vib. Acoust.* **1995**, *117*, 300–310. [[CrossRef](#)]
12. Hollkamp, J.J.; Gordon, R.W. Experiments with particle damping. In Proceedings of the 5th Annual International Symposium on Smart Structures and Materials, International Society for Optics and Photonics, San Diego, CA, USA, 16 June 1998; pp. 2–12.
13. Friend, R.D.; Kinra, V. Particle impact damping. *J. Sound Vib.* **2000**, *233*, 93–118. [[CrossRef](#)]
14. Saeki, M. Impact damping with granular materials in a horizontally vibrating system. *J. Sound Vib.* **2002**, *251*, 153–161. [[CrossRef](#)]
15. Masri, S.; Caughey, T. On the stability of the impact damper. *J. Appl. Mech.* **1966**, *33*, 586–592. [[CrossRef](#)]
16. Masri, S. Steady-state response of a multi-degree system with an impact damper. *J. Appl. Mech.* **1973**, *40*, 127–132. [[CrossRef](#)]
17. Lu, Z.; Masri, S.; Lu, X. Parametric studies of the performance of particle dampers under harmonic excitation. *Struct. Control Health Monit.* **2011**, *18*, 79–98. [[CrossRef](#)]
18. Lu, Z.; Lu, X.; Masri, S. Studies of the performance of particle dampers under dynamic loads. *J. Sound Vib.* **2010**, *329*, 5415–5433. [[CrossRef](#)]

19. Lu, Z.; Chen, X.; Zhou, Y. An equivalent method for optimization of particle tuned mass damper based on experimental parametric study. *J. Sound Vib.* **2018**, *419*, 571–584. [[CrossRef](#)]
20. Lu, Z.; Chen, X.; Zhang, D.; Dai, K. Experimental and analytical study on the performance of particle tuned mass dampers under seismic excitation. *Earthq. Eng. Struct. Dyn.* **2017**, *46*, 697–714. [[CrossRef](#)]
21. Lu, Z.; Huang, B.; Zhou, Y. Theoretical study and experimental validation on the energy dissipation mechanism of particle dampers. *Struct. Control Health Monit.* **2018**, *25*, e2125. [[CrossRef](#)]
22. Wang, Y.; Liu, B.; Tian, A.; Wei, D.; Jiang, X. Prediction methods for the damping effect of multi-unit particle dampers based on the cyclic iterations of a single-unit particle damper. *J. Sound Vib.* **2019**, *443*, 341–361. [[CrossRef](#)]
23. Wang, Y.; Liu, B.; Tian, A.; Tang, W. Experimental and numerical investigations on the performance of particle dampers attached to a primary structure undergoing free vibration in the horizontal and vertical directions. *J. Sound Vib.* **2016**, *371*, 35–55. [[CrossRef](#)]
24. Tan, J.; Michael Ho, S.C.; Zhang, P.; Jiang, J. Experimental study on vibration control of suspended piping system by single-sided pounding tuned mass damper. *Appl. Sci.* **2019**, *9*, 285. [[CrossRef](#)]
25. Ning, J.; Liang, S.Y. Inverse identification of Johnson-Cook material constants based on modified chip formation model and iterative gradient search using temperature and force measurements. *Int. J. Adv. Manuf. Technol.* **2019**, *102*, 2865–2876. [[CrossRef](#)]
26. Mia, M.; Dhar, N.R. Optimization of surface roughness and cutting temperature in high-pressure coolant-assisted hard turning using Taguchi method. *Int. J. Adv. Manuf. Technol.* **2017**, *88*, 739–753. [[CrossRef](#)]
27. Ning, J.; Nguyen, V.; Huang, Y.; Hartwig, K.T.; Liang, S.Y. Inverse determination of Johnson–Cook model constants of ultra-fine-grained titanium based on chip formation model and iterative gradient search. *Int. J. Adv. Manuf. Technol.* **2018**, *99*, 1131–1140. [[CrossRef](#)]
28. Lu, Z.; Lu, X.; Lu, W.; Masri, S.F. Experimental studies of the effects of buffered particle dampers attached to a multi-degree-of-freedom system under dynamic loads. *J. Sound Vib.* **2012**, *331*, 2007–2022. [[CrossRef](#)]



© 2019 by the authors. Licensee MDPI, Basel, Switzerland. This article is an open access article distributed under the terms and conditions of the Creative Commons Attribution (CC BY) license (<http://creativecommons.org/licenses/by/4.0/>).